



EUROfusion

EUROFUSION WPS1-PR(15) 13833

H Hoelbe et al.

Access to edge scenarios for testing a scraper element in early operation phases of Wendelstein 7-X

Preprint of Paper to be submitted for publication in
Nuclear Fusion



This work has been carried out within the framework of the EUROfusion Consortium and has received funding from the Euratom research and training programme 2014-2018 under grant agreement No 633053. The views and opinions expressed herein do not necessarily reflect those of the European Commission.

This document is intended for publication in the open literature. It is made available on the clear understanding that it may not be further circulated and extracts or references may not be published prior to publication of the original when applicable, or without the consent of the Publications Officer, EUROfusion Programme Management Unit, Culham Science Centre, Abingdon, Oxon, OX14 3DB, UK or e-mail Publications.Officer@euro-fusion.org

Enquiries about Copyright and reproduction should be addressed to the Publications Officer, EUROfusion Programme Management Unit, Culham Science Centre, Abingdon, Oxon, OX14 3DB, UK or e-mail Publications.Officer@euro-fusion.org

The contents of this preprint and all other EUROfusion Preprints, Reports and Conference Papers are available to view online free at <http://www.euro-fusionscipub.org>. This site has full search facilities and e-mail alert options. In the JET specific papers the diagrams contained within the PDFs on this site are hyperlinked

Access to long-pulse relevant edge scenarios in Wendelstein 7-X in its early phases of operation

H. Hölbe^a, T. Sunn Pedersen^a, J. Geiger^a, S. Bozhenkov^a, R. König^a,
Y. Feng^a, J. Lore^c, A. Lumsdaine^c and the Wendelstein 7-X Team

^aMax Planck Institute for Plasma Physics, Wendelsteinstr. 1, 17491 Greifswald, Germany

^bOak Ridge National Laboratory, Oak Ridge, 37831-6169, TN, USA

Abstract

Numerical calculations are presented, demonstrating that certain critical physics questions related to the plasma-wall interactions in high-performance, long-pulse operation of Wendelstein 7-X can be addressed already in the earlier (short-pulse operation) phases by appropriately adjusting the vacuum magnetic configuration. These adjustments effectively and accurately mimic long-pulse, high-performance effects due to plasma pressure and net toroidal current evolution — effects that are not directly experimentally accessible in the first operation phases, due to the limitations on pulse length and heating power. Specifically, it is shown that the Wendelstein 7-X coil system allows sufficient flexibility to accurately mimic the operational scenario for which the so-called scraper element is being considered. This enables an early and well-informed decision on whether long-pulse-capable (actively cooled) scraper elements should be built and installed.

1 Introduction

Wendelstein 7-X (W7-X) is a modular, optimized stellarator that is about to go into operation in Greifswald, Germany. It aims to demonstrate the fusion reactor relevance of the optimized stellarator concept [1]. Thus

high-performance plasma discharges, i.e. high $nT\tau$, are planned, with a heating power of currently up to 10 MW ECRH (140GHz), at a B-field of 2.5 T for up to 30 min [2]. One major issue to be studied is the efficiency and adequacy of the island divertor concept [3]. This goal is approached gradually. After an integral commissioning in 2015 [4] which only uses a limiter [5], an uncooled divertor will be used in a campaign in 2016/17 for experiments with limited pulse length before the exploration of long-pulse high-power operation will follow from 2019 on, using a fully cooled high-heat-flux (HHF) divertor [6]. The TDU and the HHF divertor have the same shape.

An important operational constraint in W7-X, or in any fusion device, is that the heat loads onto plasma facing components, in particular the divertor elements, do not exceed the engineering limits [7] set for these components. Thus, careful preparation of experimental scenarios foreseen for the HHF-phase with numerical simulations is necessary. In such simulations, scenarios have been identified that may overload parts of the HHF-divertor. This is especially the case in scenarios where the primary physics target is the investigation of configurations with optimum confinement properties, and where non-negligible net toroidal currents must be dealt with. In this connection, an additional passive safety element was proposed to miti-

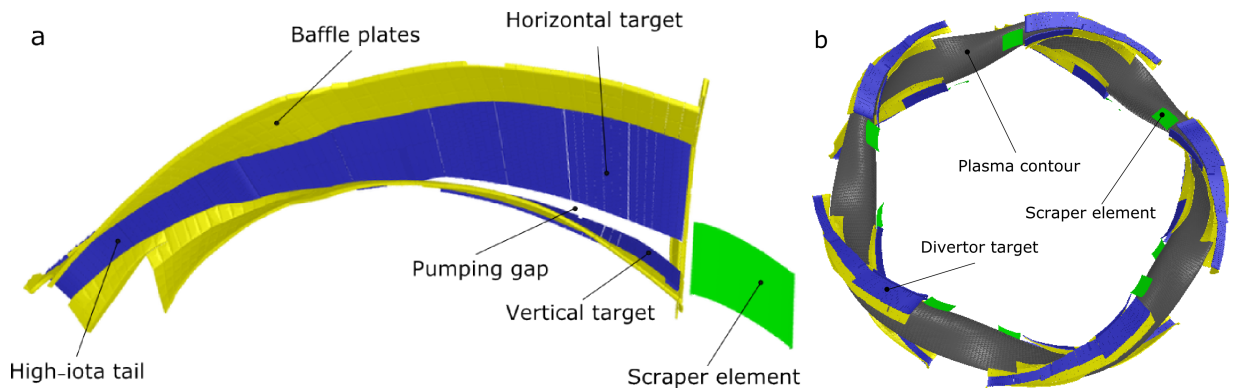


Figure 1: (a) CAD model of one W7-X divertor module as foreseen in OP1.2b with installed scraper element. Target elements are dark (online: blue), baffle plates are light grey (online: yellow) and the scraper element grey (online: green). Around the pumping gap there are the horizontal (upper part) and the vertical (below the pumping gap in the picture) targets. (b) Topview of W7-X Divertor geometry with ten divertor modules and ten SEs (cf. (a)).

gate the potential divertor operation problem. This so-called scraper element (SE), see Figure 1, could be installed in front of each divertor to intersect the magnetic flux bundles guiding convective heat to avoid the over-load situation. However, numerical simulations for discharge scenarios for which experimental comparisons are not yet available always suffer from considerable uncertainties. Therefore, an approach is necessary to assess crucial aspects of future long-pulse experiments with high-performance plasmas already during the time when only short-pulse operation with low heating power is possible. Most important is in this context the magnetic topology of the plasma edge and its consequences for operating with an island divertor. The realization of such an approach opens the possibility to experimentally explore and test mitigation strategies for potential divertor operation problems before the actual problems arise. A specific outcome of this paper are configurations developed for such exploration tests.

In Section 2 the presently planned operation phases of Wendelstein 7-X and the steps toward the island divertor are described. The “over-load” problem and the proposed scraper-element are reviewed in Sec-

tion 3. In Section 4, a strategy is presented to mimic important aspects of long-pulse, high-performance plasma experiments during shorter-pulse, lower-power operation, specifically aspects related to the edge topology and island divertor operation with the help of properly tuned vacuum magnetic configurations. The results are presented in Section 5, Section 6 the number of SE to be installed and discussed, and the conclusions are given in Section 7.

2 W7-X operation phases and the W7-X divertor

The planned operation of W7-X can be divided into separate phases of upgrades of the plasma-facing components to enable quasi-steady-state operation. The first plasma phase, the so-called operational phase 1.1 (OP1.1), starts in 2015 with five carbon limiter stripes, and no divertor. In this phase, the heating power and discharge length will be limited so as not to exceed approximately 2 MJ of total injected energy. Afterwards, the limiter is removed and with the completion of the in-vessel installations an uncooled island divertor (Test Divertor Unit or TDU) will be

installed [8]. This will be exploited in a one-year campaign from 2016 to 2017 in the operational phase 1.2 (OP1.2), the so-called TDU phase. During this phase the heating power is limited to 8 MW, and the maximum discharge time depends on the integrated heating power input because of the lack of cooling capability. The discharge time is expected to be on the order of 10 seconds for discharges heated with 8 MW. Midway through OP1.2, it is planned to install one or two un-cooled test-SEs, to verify their function, and investigate any other impact on discharge performance they may have. The parts of OP1.2 before and after the test-SE installation are referred to as OP1.2a and OP1.2b, respectively.

After OP1.2b in 2017, the un-cooled divertor and the test-SE will be removed and the actively cooled HHF-divertor will be installed, capable of withstanding a steady-state heat-load of $10 \text{ MW}/\text{m}^2$. Following the installation, operation phase 2 (OP2) is planned to start in 2019 to explore high-performance, quasi-steady-state operation (pulse length up to 30 minutes) with a heating power of up to 10 MW, and higher heating power for short pulses.

If the test-SE results are encouraging, i.e. show the necessity and compatibility of such protection elements with good divertor operation, it may be decided to build and install the 10 fully water-cooled steady-state capable SE's. The development of other strategies to deal with this problem will also be pursued. We name here only the development of experimental scenarios by investigating heating scenarios (on- vs off-axis ECRH including ECCD) and/or adjusting the magnetic configuration by further exploiting the flexibility provided by the coil system. However, it falls outside the scope of this article to analyze these here too.

3 Protection of the divertor edge

In OP1.2 and later, the plasma edge in W7-X is defined by a magnetic island chain that is intersected by divertor plates. The details of the divertor plate, the pumping gap geometry, and the location and size of this edge island chain together determine how and where the convective plasma heat loads are deposited onto the divertor plates, as well as how effectively the resulting neutrals are exhausted. The position of the edge island chain can change due to currents in the plasma, most importantly the MHD equilibrium currents that are directly or indirectly related to the normalized plasma pressure $\beta = 2\mu_0 p/B^2$, as discussed in Section 4. The plasma will therefore affect the divertor operation, in particular in high-performance discharges.

Numerical simulations of one of the potentially attractive long-pulse discharge scenarios predict unacceptably high heat loads at the ends of the divertor tiles, near the divertor pumping gap [9]. These loads would occur transiently but still last tens of seconds during the evolution of the toroidal current. The source of toroidal current in W7-X is the bootstrap current (BC), which is predicted to be relatively large for this scenario, about 43 kA. Initially, the BC is shielded by a plasma-generated counter-flowing current, but this shielding current decays gradually due to finite plasma resistivity. For the operational scenario considered, the evolution of the toroidal current takes place over hundreds of seconds.

Thus, the net toroidal current rises from near zero to about 43 kA on this time scale, with the aforementioned overload occurring at an intermediate stage, when the net toroidal current is about 22 kA. The edge topologies for different stages of the evolution of this BC-scenario (BCS) are shown in Fig-

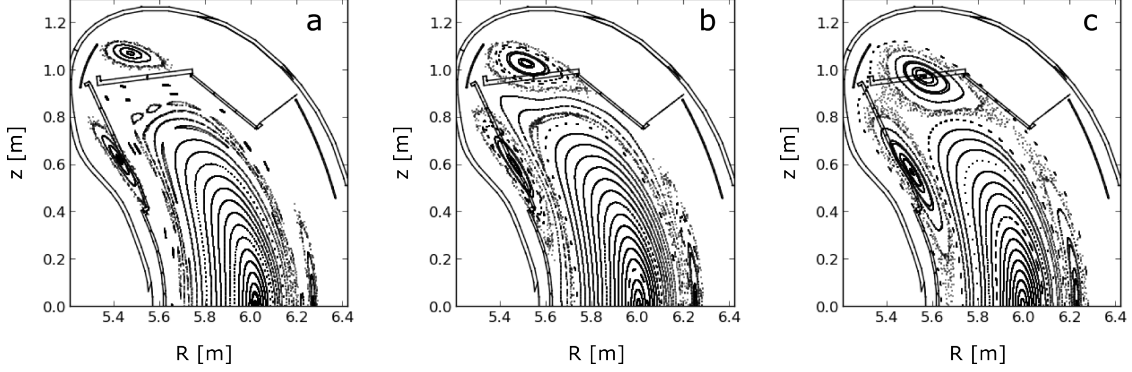


Figure 2: Poincaré plot “SE reference scenario” [9] at $\phi = 0^\circ$. BCS: (a) 0 kA, (b) 22 kA and (c) 43 kA.

ure 2.

In order to avoid this overload the installation of SEs - passive protection elements - is under consideration. A SE is an additional target plate placed in front of each divertor module (see Figure 1). It acts to intersect and eliminate (or “scrape off”) the plasma heat flux flowing along the magnetic field lines that connect to the critical locations of the HHF divertor at the pumping gap.

This SE concept was described previously in the peer-reviewed literature [10, 11]. Designed to allow for safe operation of the divertor, it could influence plasma performance negatively — for example through a significantly reduced pumping efficiency [12]. In addition, manufacturing, assembly and installation of the needed 10 SEs would require significant resources and time since they would need to be fully water-cooled.

In view of the necessary effort it would be advantageous to test the impact of the SEs on the plasma performance well in advance to allow a timely and well-informed decision on whether to have them manufactured and installed. This, however, requires experimental access to an edge topology similar to that of the scenario that has the heat load problem, the so-called “SE reference scenario”.

A test in OP1.2 would also have the ben-

efit that the tests can be performed without the danger of damage to the divertor. This is because the uncooled TDU is installed in this phase which is robust against overload scenarios and free from the danger of water leaks. However, the “SE reference scenario” with its slow time evolution is not accessible during OP1.2: As mentioned, the time limits for full power pulses are on the order of 10 seconds. Numerical calculations indicate that it would take about 40 seconds for the net toroidal current to reach the 22 kA where the problem is most prominent. It is also not guaranteed that the plasma density and heating power will be sufficient in OP1.2 to reach the parameters needed for the “SE reference scenario”. In the following we describe how an “SE reference scenario” relevant edge topology can already be generated in OP1.2, allowing the aforementioned experimental test of the potential advantages and disadvantages of an SE installation on the plasma performance.

Before proceeding, a peculiarity of the boundary topology of W7-X should be pointed out which arises in stellarators generally because of their periodicity. Structures (e.g. islands) which are resonant to a rational value of the rotational transform, i.e. comply to $t = n/m$, will close onto themselves after running around n times poloidally and m times toroidally, where m and n are the small-

est numbers forming the rational value. In W7-X, where the so-called standard configuration has a boundary- $\iota = 1$, this means that boundary islands close onto themselves after one toroidal and one poloidal turn. However, assuming strict 5-fold periodicity implies that a structure closing onto itself after one toroidal and one poloidal turn must be present five times. Because of this, five independent islands are forming the separatrix at the boundary rotational transform of $\iota = 1$ which is sometimes emphasized by writing $\iota = 5/5$. Periodicity also implies that resonant ι -values ($\iota = n/m$) must have n as a multiple of 5. In consequence, if the denominator m is not a multiple of 5, for example $\iota = 5/6$ or $5/4$, the so-called low-iota or high-iota cases, the islands seen in a Poincaré plot (6 or 4) in one poloidal cross section are helically connected, i.e. one island chain only. Periodicity breaking error fields or non-periodic in-vessel installations have to be given special attendance if $\iota = 5/5 = 1$.

4 Development of test scenarios

The approach taken here is to match the edge topology of the different stages of the evolution of the net plasma current by adjusting the coil currents. That is, the same edge magnetic topology is mimicked as closely as reasonably possible in a zero- β , zero-toroidal-current (i.e., vacuum) configuration as would exist in a high- β , finite-toroidal-current equilibrium using the flexibility provided by the main and auxiliary coil systems of W7-X [2]. Because the heat load distribution on the different divertor parts is the property of interest, the "SE reference scenario" will be assessed by a sequence of specially designed vacuum configurations which reproduce the important properties of the heat load distributions of the different stages of the "SE-

reference scenario". Hence, a perfect match of the magnetic configuration in total is not the goal but to reproduce the effects of the boundary topology changes on the load distribution to the different divertor parts. Thus, a configuration with finite β and/or a net-toroidal current is seen as equivalent to a vacuum configuration in this context if their relative heat load distributions on the different divertor parts are the same. A comparison of these heat load distributions will be used to calibrate the coil current changes to mimic the different plasma current effects.

There are two distinct plasma current effects on the configuration in W7-X, and they evolve on different time scales. One is due to the perpendicular diamagnetic current density \vec{j}_\perp needed for the basic MHD force balance:

$$\nabla p = \vec{j}_\perp \times \vec{B} \quad (1)$$

Because in toroidal magnetic configurations this current is not divergence free, there is a parallel current density part connected with \vec{j}_\perp , the so-called Pfirsch-Schlüter (PS) current, which affects the equilibrium but does not contribute to the net toroidal current. In a tokamak, the sum of the diamagnetic and PS currents does produce a net toroidal current, but in a current-free stellarator it does not [13]. The other one, the net toroidal current, is due to the bootstrap current as well as the induced shielding currents which appear in response to the bootstrap current. The diamagnetic current and the PS current together evolve on the time scale of the changes in ∇p i.e., on the time scale of the energy confinement time (of order 200 ms in W7-X) whereas the net toroidal current evolves on the much longer plasma self-screening time, also known as the L/R time, which will be on the order of 20–40 seconds for high performance scenarios. Currents may also be induced in conducting structures surrounding the plasma, e.g. the plasma vessel itself. These decay, however,

on time scales of less than 50 ms in W7-X. Thus, they will not play an important role for the slowly evolving equilibrium effects that are important for the divertor operation, and they will consequently be ignored in the following. We will refer to the effects due to the diamagnetic current and the PS current collectively as β effects. The BC and the self-shielding plasma response to it together entail the net toroidal current effects. Because of the very different time scales on which the β -effect currents and the net toroidal currents evolve, they will be assessed independently.

4.1 Effect of plasma β

The diamagnetic part of the equilibrium currents is mostly poloidal and its effect on the equilibrium is therefore small since it "competes" with the mostly poloidal current of the main superconducting coils of W7-X. The PS currents generate mainly poloidal field components of the same magnitude as the vacuum field, hence with a stronger effect on the internal flux surfaces (axis shift and change in rotational transform) as well as on the structure of the magnetic field outside the plasma — i.e. the boundary islands. Figure 3 shows the latter effect in a sequence of Poincaré plots of magnetic fields derived from VMEC/Extender [15], [16], [17] calculations [14] with increasing β values. Generally, the island width (radial width, not the poloidal extent given by the spacing of the x-points) increases with β ; this can be best observed in the change in the upper island of the bean-shaped cross section. Furthermore, with increasing β the field around the x-points/separatrix tends to become stochastic [17],[18],[19].

In order to mimic these β -effects, neither the 50 non-planar coils nor the 20 planar coils of the main coil system are suited, since changing the currents in these coils tends to change many other important parameters si-

multaneously (rotational transform, toroidal mirror field component and/or horizontal plasma position) in addition to the island width.

However, the so-called sweep coils, a set of 5x2 stellarator-symmetric coils inside the vacuum vessel which all have independent power supplies, can be used in a stellarator symmetric operation mode to control the island size without substantially changing the rest of the topology. This method does not allow a perfect match to the island size at finite β , but it is sufficiently close enough to generate an interaction between the island chain and the plasma-facing components which is very similar to that at finite β . This suffices for many purposes, including the ability to mimic the "SE reference scenario".

4.2 Net toroidal current

The optimization to a near-zero BC was done for one specific configuration in W7-X. Non-negligible BC exists for other interesting configurations and discharge scenarios. Nevertheless, the BC in W7-X is generally an order of magnitude smaller than in a tokamak or classical stellarator of similar size and rotational transform. Due to the low magnetic shear, even this rather small BC can have a significant impact on the edge islands and the island divertor operation. According to transport simulations for different magnetic configurations achievable in W7-X, better confinement is usually accompanied by an increasing bootstrap current. Thus, in order to take advantage of best-confinement configurations, a modest BC might have to be accepted with the result of a changed edge topology and in turn changed heat load patterns on the divertor (see Figure 2 and as discussed in Section 3), even if this requires the development of mitigation strategies to allow for safe divertor operation.

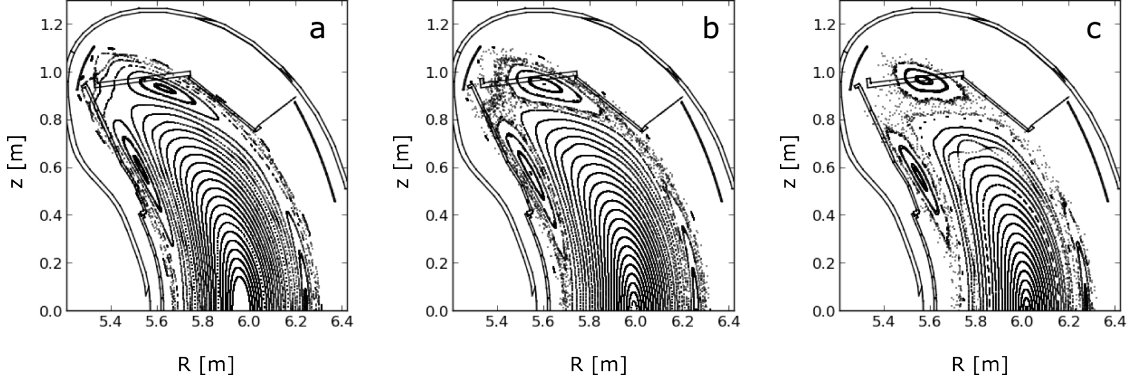


Figure 3: β scan of standard configuration (no BC included). Poincaré plots at $\phi = 0^\circ$. Average β : a: 0.65%, b: 2% and c: 3.4%. Magnetic fields calculated with VMEC and Extender [14].

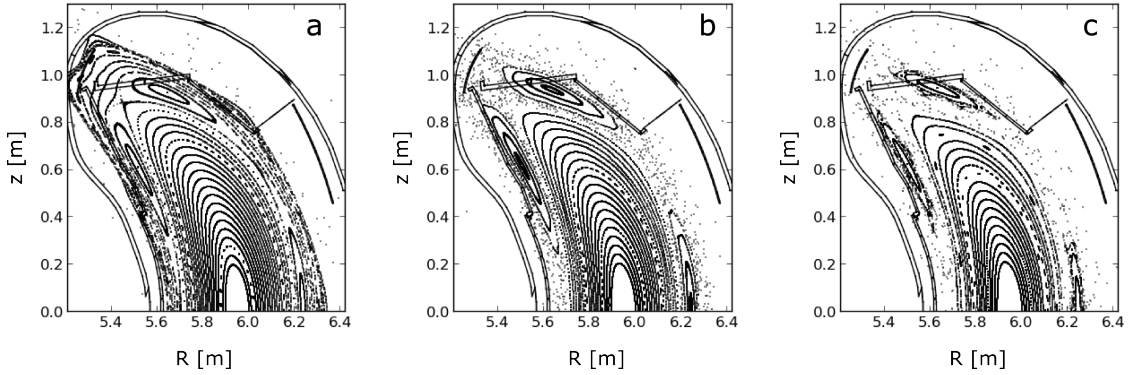


Figure 4: Sweep coil current scan (vacuum configuration). Poincaré plots at $\phi = 0^\circ$. Vacuum magnetic fields: Modular coil currents ($I_1 = \dots = I_5 = 1.0$), planar coil currents ($I_A = I_B = 0$) and sweep coil currents for island size variation: (a) $I_{s1} = 0, I_{s1} = 0$. (b) $I_{s1} = -0.02, I_{s1} = 0.02$. (c) $I_{s1} = -0.04, I_{s1} = 0.04$.

The net toroidal current first and foremost affects the rotational transform. One of the main purposes of the 20 planar coils is to change the rotational transform ι , without strongly affecting the other properties of the equilibrium. These coils can therefore be used to mimic the effect of a net-toroidal current when none is present. The achievable match is not perfect; the changes in magnetic shear, $d\iota/d\psi$, cannot be matched while simultaneously matching the changes in ι at the plasma edge (ψ is the toroidal magnetic flux). Nevertheless, for the configurations studied here the effect due to the mismatch in shear is negligible.

Figure 5 shows the movement of the boundary islands with respect to the divertor when tuning the rotational transform up and down from its boundary value of 1.0 in the standard configuration (same currents in the modular coils, no other coils used), using the planar coils. Comparing this sequence with the “SE reference configuration” with increasing net toroidal current (Figure 2) shows that the islands move inward in the same way.

Thus, broadly speaking, vacuum field configurations can mimic configurations with finite β and finite net toroidal current by adjusting the currents in the sweep coils and the planar coils.

4.3 Calibration

In order to be able to adjust the coil currents properly so that the vacuum or low- β configurations are equivalent in the previously mentioned definition, i.e. equivalence of heat load pattern distribution on the different divertor parts, we need to provide a mapping. Thus we assess the relative heat loads on the different divertor parts (targets, baffles, SE) in a global way, i.e. not the local distribution on these parts. For this, we use a field line diffusion approach that simulates the trans-

port perpendicular to the magnetic field [20]. For this, field lines, starting at the separatrix, are traced. After a random distance a random step perpendicular to the field line is performed and the tracing is continued starting from the new point. If a component (for example the divertor target plate) is hit the point of impact is recorded and the field line tracing procedure is started again with a new point at the separatrix. The number of impact points per area divided by the total number of field lines traced is used as a figure of merit for the fraction of the heat load hitting this area. Later, in Section 5, a cross-check will be done by inspecting the local strike line patterns.

The coil current values given in the following have to be interpreted as relative total currents of the respective coils, i.e. the current per winding times the number of windings of the coil with respect to a normalization current whose special value is not relevant in the current context. Thus, the so-called standard configuration has the same relative currents for the five modular coils and zero for all others. A configuration is described by the full set of relative coil current values, i.e. for all modular coils, planar coils and control coils.

4.3.1 β calibration

Figure 6 compares the distribution of the heat loads on the different divertor components (including the SE) resulting from a β -sequence of MHD-equilibria with the ones resulting from vacuum fields obtained by properly adjusting the currents in the sweep coils. As seen, the redistribution of the heat loads with β can be well reproduced by an appropriate adjustment of the sweep coil currents.

Note, the “SE reference scenario” has a β -value of 2.7%. The sweep coil current to imitate this β -value is used later for the OP1 mimic configurations (Coil currents in Table

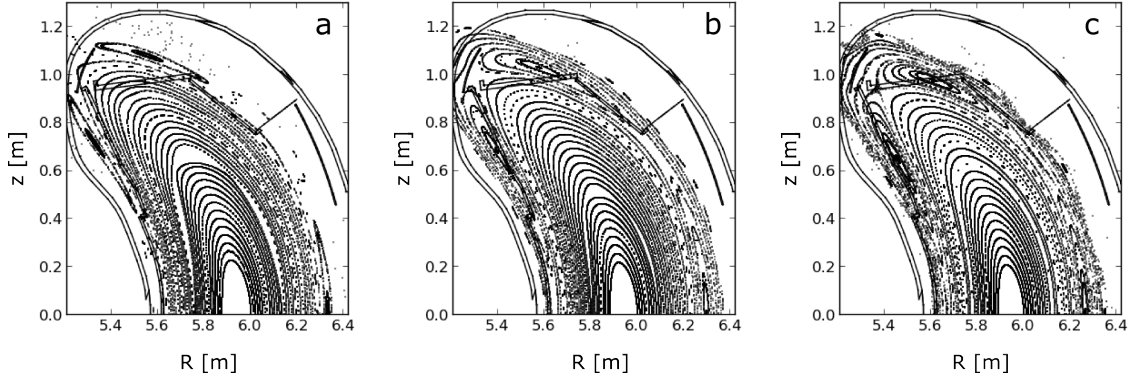


Figure 5: Poincaré plot of iota scan (vacuum configurations) at $\phi = 0^\circ$. Modular coil currents ($I_1 = \dots = I_5 = 1.0$) and planar coil currents (I_A, I_B) for controlling the rotational transform: (a) $I_A = 0.12, I_B = 0.12$. (b) $I_A = 0.08, I_B = 0.08$. (c) $I_A = -0.04, I_B = -0.04$.

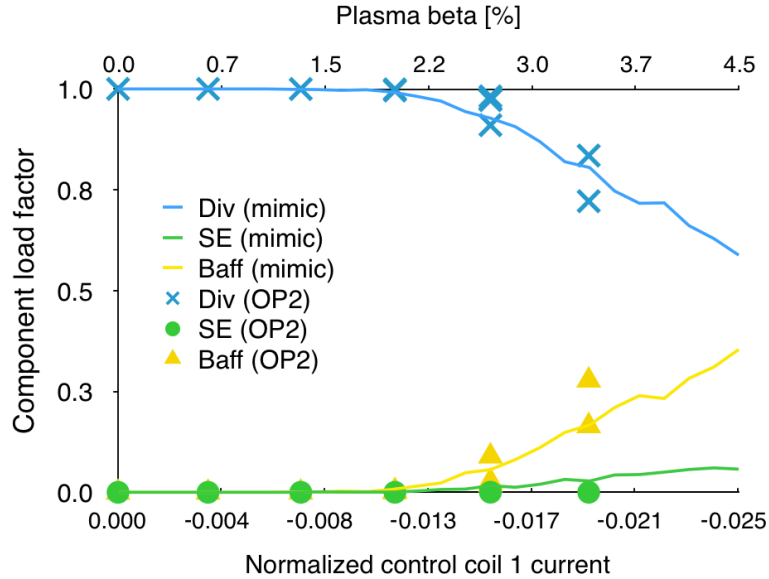


Figure 6: Mimicking plasma beta effect with magnetic coils. Lines: Control coil current scan (vacuum configurations). Crosses/Circles/Triangles: MHD-equilibrium calculation for different beta values. Each equilibrium calculation was done for different values of plasma radius. Y-Axis shows relatively head load fraction of total heat load on specific component for the specific configuration. The current of control coil 2 is minus the current of control coil 1. Currents modular coils = 1, planar coils current = 0. To archive a main field of 2.5 T the normalized currents have to be multiplied by 1.47 MA.

1).

4.3.2 Iota calibration

Finite current in the planar coils is used in vacuum configurations to imitate the effect of the net-toroidal current. Figure 7, shows the change of the heat loads on the different components for the net-toroidal current sequence in the “SE reference scenario” as well as for the vacuum configurations obtained by adjusting the currents of the planar coils. With an appropriate mapping of the values of the coil current to the ones of the net-toroidal current a remarkably good match of the heat loads can be achieved (compare 7c). The Poincaré plots of the configurations which mimic the 0 kA, 22 kA and 43 kA cases are shown in Figure 8. Note that the upper island is intersected by the horizontal diverter plates at similar positions as in the “SE reference configurations” (compare to Figure 2).

Both effects, β - and net-toroidal current, can be combined to simulate the expected heat load distribution of the “SE reference scenario” during the evolution in a long-pulse discharge. Table 1 gives the sequence of corresponding relative coil currents to reproduce the global heat load distribution on the different divertor parts with vacuum fields.

5 Results

5.1 Strike-line pattern

Up to this point, the details of the strike-line patterns have been ignored with the focus being on the integral power flux onto the components. However, for some locations it is necessary that also the strike-line patterns are similar. This is especially important for the loads near the pumping gap and the loads onto the SE, since the details of their distribution will

have a strong influence on the pumping efficiency of the neutrals created on the targets by the outflow of plasma.

Figure 9 compares the strike line pattern of the configuration of the SE-reference scenario with 22 kA (for which an overload at the pumping gap would be expected without the SE) with the pattern generated by the corresponding mimic vacuum configuration. Note that the shape of the pattern on the SE is very similar for the two cases, although for the vacuum case, the hot-spot at the front (upper part in picture) is somewhat more intense. The heat-flux to the pumping gap is at the same level for the two configurations, but for the mimic vacuum field, the horizontal target plate (right part of TDU in picture) is loaded somewhat more.

The strike line pattern for the stationary configuration with 43 kA is shown in Figure 10 along with the corresponding mimic configuration. In this case, the heat flux to the SE is also very similar for the two configurations. The heat load pattern of the full scenario calculation has one more strike line on the horizontal target plate than its corresponding vacuum configuration. This strike line is caused by the additional changes in the island shape due to the β -effects. With the available vacuum field coil set it was so far not possible to simultaneously provide a perfect match of the changes in the strike line patterns due to β and net-toroidal current everywhere. However, since the additional strike line is located far away from the pumping gap, its impact on the pumping efficiency is considered to be very small, so that investigations of the effect on the pumping efficiency should not be affected.

5.2 Further use of the configurational flexibility

The approach described here opens up more possibilities for generating other test-

Table 1: Coils currents to mimic the “SE reference scenario” in OP1.2. Planar coils used to mimic toroidal current evolution, sweep coils for mimicking the β effect of $\beta = 2.7\%$. Modular coils same as the “SE reference scenario”.

ID	BC	I_A	I_B	I_{s1}	I_{s2}	I_1	I_2	I_3	I_4	I_5
6	0 kA	0.220	-0.080	-0.015	0.015	0.96	0.95	0.97	1.07	1.08
11	11 kA	0.195	-0.105	-0.015	0.015	0.96	0.95	0.97	1.07	1.08
16	22 kA	0.170	-0.130	-0.015	0.015	0.96	0.95	0.97	1.07	1.08
21	32 kA	0.145	-0.155	-0.015	0.015	0.96	0.95	0.97	1.07	1.08
26	43 kA	0.120	-0.180	-0.015	0.015	0.96	0.95	0.97	1.07	1.08

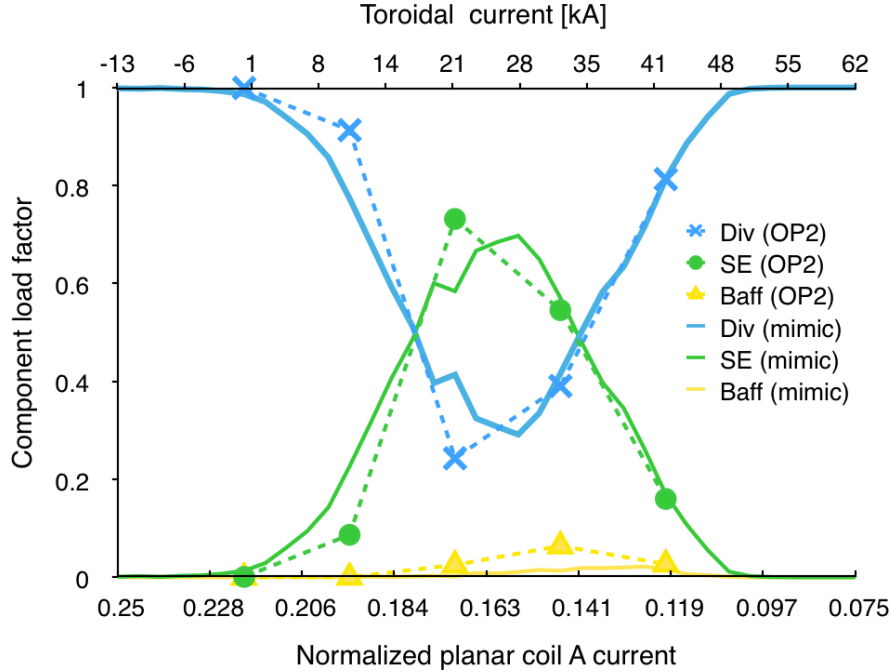


Figure 7: Mimicking the “SE reference scenario” evolution. Lines: planar coil current scan, vacuum configuration. Crosses/Circles/Triangles: MHD-equilibrium calculation of different toroidal currents of the “SE reference scenario”. Y-Axis shows relatively head load fraction of total heat load on specific component for the specific configuration. Mimic configurations planar coil B current is planar coil A current minus 0.3. Mimic configurations: Control coil 1 = -0.015, Control coil 2 current = 0.015. Modular coil currents: $I_1 = 0.96$, $I_2 = 0.95$, $I_3 = 0.97$, $I_4 = 1.07$, $I_5 = 1.08$. To archive a main field of 2.5 T the normalized currents have to been multiplied by 1.47 MA. See table 1 for mimic configuration details.

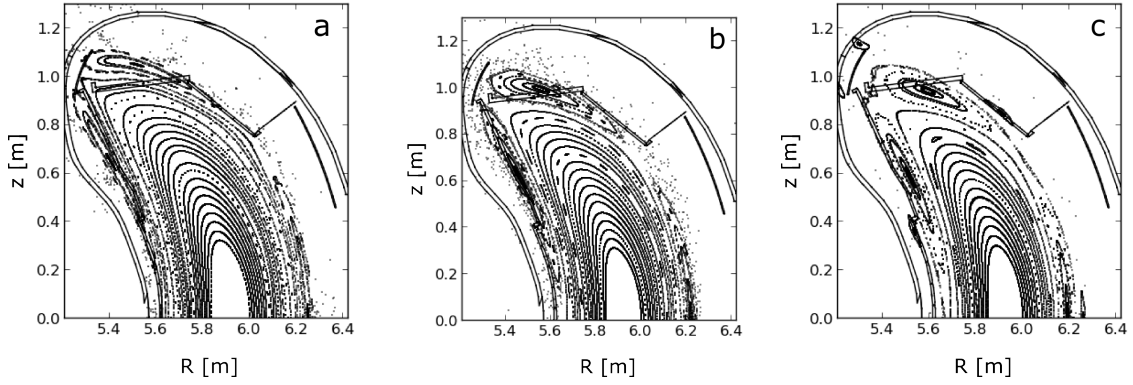


Figure 8: Poincaré plots of vacuum fields of mimic configurations at $\phi = 0^\circ$. Currents to mimic: (a) 0 kA, (b) 22 kA and (c) 43 kA.

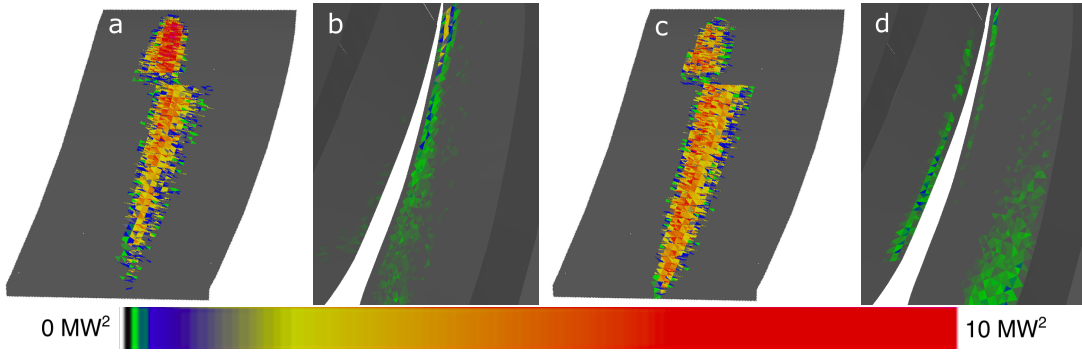


Figure 9: Strike line patterns for the 22 kA configuration, as well as for the corresponding OP1 mimic configuration. (a) SE, mimic configuration/OP1, (b) Divertor, mimic configuration/OP1, (c) SE, "SE reference scenario"/OP2, (d) Divertor, "SE reference scenario"/OP2.

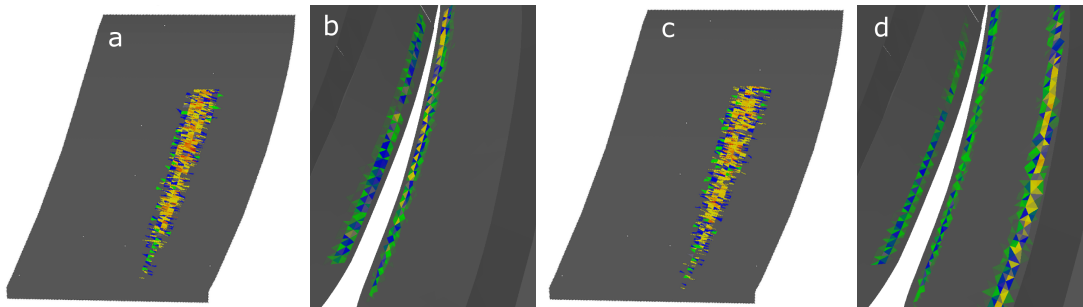


Figure 10: Strike line patterns for the 43 kA steady state configuration, as well as for the corresponding OP1 mimic configuration. (a) SE, mimic configuration/OP1, (b) Divertor, mimic configuration/OP1, (c) SE, "SE reference scenario"/OP2, (d) Divertor, "SE reference scenario"/OP2.

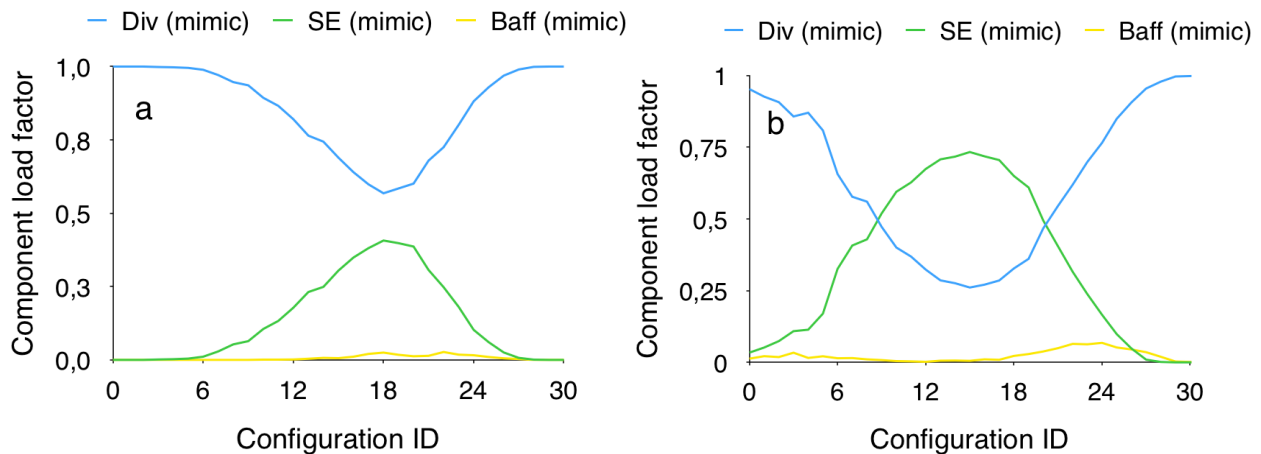


Figure 11: Alternative TDU-SE test scenarios. (a) Reduced heat flux at the SE in a less inward shifted configuration. (b) Increased heat flux at the SE for a configuration with increased mirror ratio.

configurations. Due to the limits that are set for OP1.2 with respect to the combination of discharge length and heating power it might be useful to be able to additionally vary the heat load on the SE via adjustments of the magnetic configuration. This might, for example, help to get a heat load on the SE which or whose effects can be better assessed by the diagnostic systems. Here we only show two examples of decreasing or increasing the heat load by such means.

First, the use of the planar coils to vary the horizontal plasma position makes it possible to vary the heat load onto the SE without changing the input heating power. Figure 11a shows the heat loads on the different divertor parts for the mimic-SE-reference configuration being slightly shifted outward with the effect of reducing the load on the SE. This, on the other hand, means that there is a higher risk for overloading the baffle plates on the outward side.

Second, the coil currents in the modular coils can be used to change the magnetic field strength along the axis which is usually larger at the bean-shaped planes (shown in the Poincaré plots in the paper) and smaller in the planes in between. Figure 11b shows that by decreasing the field strength between

the bean-shaped planes, i.e. increasing the mirror field, it is possible to increase the relative heat load on the SE in the same toroidal current scan as in Figure 11a.

6 Two versus 10 scraper elements

As already pointed out, one or two TDU-SE elements will be installed after the first half of the experimental campaign OP1.2, i.e. after OP1.2a. The reduced number - the full set would require 10 SEs - is to limit the effort in manufacturing and in assembly for this first test. Although this introduces an asymmetry in the heat loads, it also offers opportunities for valuable comparisons. On the one hand, it will be possible to compare configurations and discharges without and with SEs installed (OP1.2a vs OP1.2b). On the other hand, the reduced set of SEs in OP1.2b allows a comparison of shielded and unshielded divertor units in the same discharge and configuration. However, for the latter symmetry and periodicity of the magnetic field and of the in-vessel components are crucial conditions, but this will and needs to be investigated in any case.

In case that two TDU-SE elements are in-

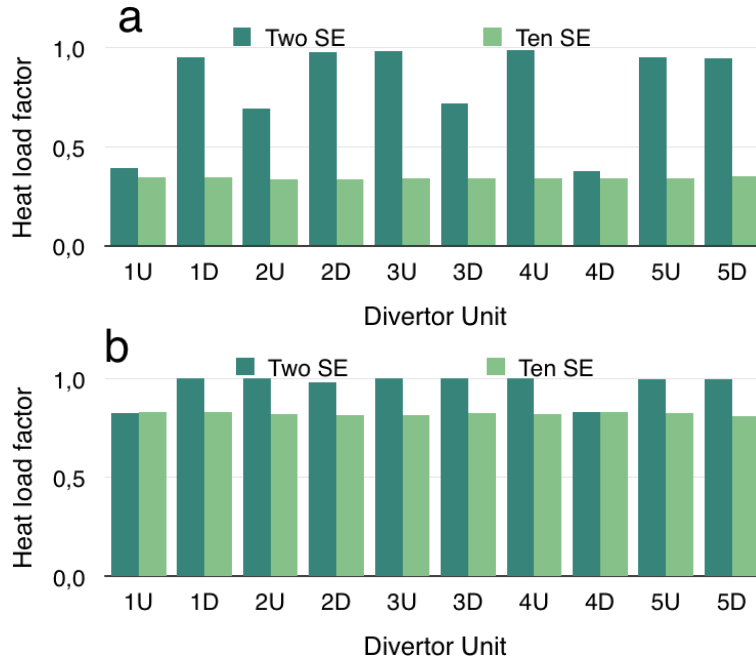


Figure 12: Load onto the different TDU modules comparing reduced (2) and full (10) SE-set. Naming of divertor units: XY with X=number of machine module (1,...,5) and Y=location within the respective module (U/D=upper/lower divertor unit). (a) OP1.2 configuration for mimicking 22 kA toroidal current. (b) OP1.2 configuration for mimicking 43 kA toroidal current.

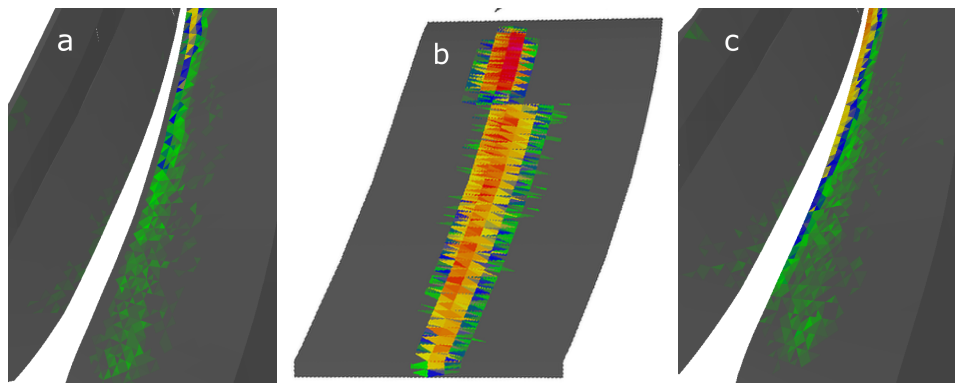


Figure 13: 22kA mimic configuration. Heat load patterns at different divertor parts with only two SE: (a) shielded pumping gap (divertor unit with adjacent SE), (b) SE, (c) unshielded pumping gap (divertor unit without adjacent SE).

stalled, the boundary- ι value of 1 for the configurations we consider here and the argument of stellarator-symmetry suggests to install them 180° toroidally and poloidally separated from each other (one at the top, one at the bottom divertor). For configurations with a boundary-value of $\iota = 1$, these two locations are magnetically linked and will shadow each other (and their respective two divertor units). In a full installation there would be 5 (periodicity) such linked divertor and SE combinations. Thus, it is important to know how accurately such a partial installation (one or two SE) can be used to assess how the full system of ten scraper-elements will behave in later operation. We will focus on two time points during the time evolution of the “SE reference scenario”: i.e. when 22 kA of net toroidal current is reached (design point of the SE to avoid the overload of the divertor at the pumping gap) and when 43 kA of net toroidal current is reached - the steady state situation. To investigate the situation to be expected in OP1.2, we base our analysis on the two corresponding mimic vacuum configurations. An extrapolation of the obtained results in this model to what is expected in OP2 with a full set may be nevertheless justified on the basis of the prior results, namely, that the heat load patterns and the expected pumping efficiencies between the mimic configurations and their OP2 counterparts can be expected to be essentially similar. Because for the considered magnetic configurations the boundary structures have the same periodicity as the divertor units, the ones without a SE installed adjacent to them see only a negligible influence from scraper elements installed somewhere else. The heat load onto such units decreases by only 1.5%. The two divertor units with adjacently installed SEs see a similar heat load reduction whether two or ten SEs are installed. The additional heat load reduction when going to the full set of SEs is only 10-12% of the already reduced heat

loads for the 22 kA-configuration and almost no effect is seen for the 43 kA-configuration. The results are shown in detail in Figure 12.

The heat loads onto the TDU SEs themselves are, however, substantially different whether two or ten are installed. The heat load onto one of ten SE is about 35% smaller compared with the heat load at one SE out of two. The reason for this is that the SEs do not only shield their adjacent TDU-module and their magnetically connected counterpart but also SEs in other periods. Also, the effect on the TDU-modules is always distributed onto ten modules (or eight if one considers the unshielded ones), while for the SEs the distribution of the load varies from two to ten. In addition, the strike line pattern on the SE is extended in the direction away from the divertor unit. See Figure 13.

7 Conclusion

We have shown that topological changes in the edge region due to β and due to net toroidal currents can be mimicked remarkably accurately with near-zero β , near-zero bootstrap current configurations, using the existing coil set of W7-X. Specifically, effects caused by the MHD-equilibrium currents can be mimicked by adjusting the currents in the sweep coils, and effects caused by the net-toroidal current can be mimicked by adjusting the currents in the planar coils. Thus it seems possible to experimentally investigate aspects of the interaction between plasma and divertor expected in some high-performance plasma scenarios accessible only in the later experimental phase OP2 (2019 and beyond) already in the earlier experimental phase OP1.2 (2016/17). Moreover, this allows for an OP1.2 test program for the SEs to assess their potential advantages and disadvantages, despite them being designed to mitigate a possible divertor overload sce-

nario that would only be interesting for quasi-steady-state operation, i.e. for very long discharges, in OP2. Most notable is that for a physics assessment of the effects of the full set of 10 SEs only a subset of two is sufficient to evaluate their effectiveness in configurations with $\iota = 1$, thus allowing for significant resource savings. Additionally, the results of such a program can broaden the basis on which a final decision on whether to manufacture and install a fully cooled SE-set during OP2. It should be noted, however, that the details of the heat load patterns will be somewhat different between a situation with ten or with two SEs. Nevertheless, their shielding effect can be assessed accurately enough experimentally and their impact on the pumping-efficiency is expected to be similar enough to be applicable for the other cases. Finally, it should be recalled that additional efforts in the scenario development are performed to explore alternatives for the SE-reference scenario avoiding the need of protective measures for the pumping gap.

Acknowledgement

This work has been carried out within the framework of the EUROfusion Consortium and has received funding from the Euratom research and training programme 2014-2018 under grant agreement No 633053. The views and opinions expressed herein do not necessarily reflect those of the European Commission

References

- [1] Grieger G, Lotz W, Merkel P, Nührenberg J, et al "Physics optimization of Stellarators" 1992 Phys. Fluids B 4, 2081
- [2] J.Geiger et al. "Physics in the configuration space of W7-X" 2015 Plasma Phys. Control. Fusion 57 014004
- [3] Grigull P, McCormick K, Baldzuhn J et al "First island divertor experiments on the W7-AS stellarator" 2001 Plasma Phys. Control. Fusion 43, A175
- [4] Bosch H.S, Brakel R, Gasparotto M, et al "Transition From Construction to Operation Phase of the Wendelstein 7-X Stellarator", 2014 IEEE Transactions on Plasma Science, 42, 3, 432-438
- [5] Bozhenkov S.A, Effenberg F, Feng Y, et al "Limiter for the early operation phase of W7-X" 2014 41st EPS Conference on Plasma Physics, P1.080,
- [6] Renner H, Sharma D, Kießlinger J, Boscary J, et al "Physical Aspects and Design of the Wendelstein 7-X Divertor", 2004 Fusion Sci. Technol., 46, no.2, 318-326
- [7] Boscary J, Peacock A, Friedrich T, et al "Design improvement of the target elements of Wendelstein 7-X divertor", 2012 Fusion Engineering and Design, 87 7-8, 1453-1456
- [8] Peacock A, Greuner H, Hurd F, et al "Progress in the design and development of a test divertor (TDU) for the start of W7-X operation", 2009 Fusion Engineering and Design, 84, 7-11, 1475-1478
- [9] Geiger J, Beidler C.D, Drevlak M, et al "Effects of Net Currents on the Magnetic Configuration of W7-X" 2010 Contrib. Plasma Phys., 50, 8, 770-774
- [10] Lumsdaine A, Boscary J, Clark E "Modeling and Analysis of the W7-X High Heat-Flux Divertor Scrapper Element", 2014 IEEE Transactions on Plasma Science, Part 1
- [11] Lore J.D, Andreeva T, Boscary J, et al "Design and Analysis of Divertor Scrapper Elements for the W7-X Stellarator" 2014 25th Symposium on Fusion Engineering (SOFE 2013). IEEE.

- [12] H. Hölbe "EMC3 simulations of OP2 SE operation" To be submitted to Nuclear Fusion
- [13] Helander P., "Theory of plasma confinement in non-axisymmetric magnetic fields", 2014, Rep. Prog. Phys., 77, 087001
- [14] Geiger J, Private communication 2013
- [15] Hirshman S.P, Whitson J.C "Steepest-descent moment method for three-dimensional magnetohydrodynamic equilibria" 1983 Phys. Fluids, 26, 12, 3553-3568
- [16] Hirshman S. P, van Rij W. I, Merkel P, "Three-dimensional free boundary calculations using a spectral Green's function method" 1986 Comput. Phys. Commun., 43, 1, 143-155.
- [17] Drevlak M, Monticello D, Reimann A, "PIES free boundary stellarator equilibria with improved initial conditions" 2005 Nucl. Fusion, 45, 7, 731-740.
- [18] Strumberger E "Finite- β magnetic field line tracing for Helias configurations" 1997 Nucl. Fusion 37, 1, 19-27
- [19] Renner H, Boscary J, Greuer H, et al "Divertor concept for the W7-X stellarator and mode of operation" 2002 Plasma Phys. Control. Fusion 44 1005
- [20] Bozhenkov S.A, Geiger J, Grahl M, et al "Service oriented architecture for scientific analysis at W7-X. An example of a field line tracer" 2013 Fusion Engineering and Design, 88, 11, 2997-3006
- [21] Werner A, Endler M, Geiger J, Koenig R. "W7-X magnetic diagnostics: Rogowski coil performance for very long pulses." 2008 Rev Sci Instrum. 79